Imaging the electromechanical activity of the heart in vivo

Jean Provost[a], Wei-Ning Lee[a], Kana Fujikura[b], and Elisa E. Konofagou[a,b,1]

[a]Department of Biomedical Engineering, Columbia University, New York, NY 10027; and [b]Department of Radiology, Columbia University, New York, NY 10032

Edited by Charles S. Peskin, New York University, and approved April 7, 2011 (received for review August 19, 2010)

Cardiac conduction abnormalities remain a major cause of death and disability worldwide. However, as of today, there is no standard clinical imaging modality that can noninvasively provide maps of the electrical activation. In this paper, electromechanical wave imaging (EWI), a novel ultrasound-based imaging method, is shown to be capable of mapping the electromechanics of all four cardiac chambers at high temporal and spatial resolutions and a precision previously unobtainable in a full cardiac view in both animals and humans. The transient deformations resulting from the electrical activation of the myocardium were mapped in 2D and combined in 3D biplane ventricular views. EWI maps were acquired during five distinct conduction configurations and were found to be closely correlated to the electrical activation sequences. EWI in humans was shown to be feasible and capable of depicting the normal electromechanical activation sequence of both atria and ventricles. This validation of EWI as a direct, noninvasive, and highly translational approach underlines its potential to serve as a unique imaging tool for the early detection, diagnosis, and treatment monitoring of arrhythmias through ultrasound-based mapping of the transmural electromechanical activation sequence reliably at the point of care, and in real time.

strain | electromechanical coupling

The heart is an electromechanical pump that requires to first be electrically activated in order to contract. In the normal heart, action potentials are spontaneously generated by the sinus node in the right atrium and propagate through a specialized conduction system before reaching the cardiac muscle. The depolarization of a cardiac muscle cell, or myocyte, is followed by an uptake of calcium, which triggers contraction (1) after an electromechanical delay of a few milliseconds (2, 3). In the clinical setting, the electrical and mechanical functions of the heart are typically evaluated separately. The cardiac electrical function is usually assessed using an electrocardiogram (ECG) or catheter-based mapping systems. New noninvasive imaging technologies based on body surface potentials (4–6), cavity potentials (7), or magnetic fields (8) are also being developed. Methods used to measure the cardiac electrical activity typically ignore the cardiac motion. On the other hand, the cardiac mechanical function can be assessed using ultrasound or magnetic resonance (MR) techniques, but at such large time scales that the electrical activation occurs within one time frame and is hence ignored. In the laboratory, the cardiac electromechanical coupling has been and remains the topic of extensive research at the cellular level in vitro (3), in cardiac simulation models (9–12), and at the tissue level in animal models in vivo (2, 13–15). To perform such studies, it is necessary to map the electromechanics of the heart (i.e., the deformations occurring at the time scale of the electrical activation). For example, in refs. 13 and 14, a linear relationship between the electrical activation and contraction onset in healthy, paced, canine hearts was found in vivo, indicating the use of electromechanical mapping techniques to identify, for example, ectopic sites (14). To date, no imaging method can noninvasively provide sufficient temporal resolution, accuracy, or field of view to reliably map the electromechanics of the heart in vivo.

In this paper, an entirely ultrasound-based imaging technology, electromechanical wave imaging (EWI), is described and evaluated with respect to its capability of mapping the electromechanics of the heart in vivo. EWI can map the electromechanical activity in all four heart chambers at a very high temporal resolution (approximately 2 ms), noninvasively and with real-time feedback. At such a high temporal resolution, a number of phenomena occurring in the temporal vicinity of the electrical activation, including the onset of contraction resulting from the electrical activation, as well as the opening and closing of the valves and ventricular hemodynamics, can be separated in space and time, mapped and quantified (16). At the tissue level, the depolarization of myocardial regions triggers electromechanical activation (i.e., the first time at which the muscle transitions from a relaxation to a contraction state). Spatially, this electromechanical activation forms the electromechanical wave (EW) front that follows the propagation pattern of the electrical activation sequence.

As of today, no imaging method currently used in the clinic has been capable of mapping the EW. The EW lasts approximately 60 to 100 ms and requires a resolution of a few milliseconds (e.g., 2–5 ms) to generate precise activation maps. Moreover, the regional interframe deformation that has to be measured at these frame rates is very small (approximately 0.25% at a 2-ms temporal resolution) and requires a highly accurate strain estimator. Modalities such as standard echocardiography or MR tagging cannot detect the EW, because the time required to acquire a single image is similar to the duration of the entire ventricular depolarization. Effectively, because standard echocardiography was originally designed to assess the overall mechanics of specific cardiac segments over the entire heart cycle, images are typically acquired every 20–30 ms. Full-view speckle tracking techniques such as tissue Doppler or strain rate imaging have achieved motion estimation with high spatial resolution but require relatively low frame rates. Higher temporal resolution and motion estimation accuracy can be achieved using, e.g., motion mode, but at the expense of a very narrow field of view that does not allow spatial assessment of the propagation. Strain mapping methods based on MR imaging (MRI) in humans are not real time, and their frame rates are typically smaller than in echocardiography, although temporal resolution on the order of 15–20 ms has been achieved (17, 18).

EWI is currently implemented at frame rates up to 500 frames per second (fps) (corresponding to a 2-ms temporal resolution), which is five times higher than standard echocardiography while providing the same large field of view. At those frame rates, EWI uses radio frequency (RF)-based cross-correlation, a motion

Author contributions: J.P., W.-N.L., and E.E.K. designed research; J.P., W.-N.L., and K.F. performed research; J.P. and W.-N.L. analyzed data; and J.P. and E.E.K. wrote the paper.

The authors declare no conflict of interest.

This article is a PNAS Direct Submission.

[1]To whom correspondence should be addressed. E-mail: ek2191@columbia.edu.

This article contains supporting information online at www.pnas.org/lookup/suppl/doi:10.1073/pnas.1011688108/-/DCSupplemental.

estimation method that can be up to ten times more accurate than brightness mode (B mode)-based speckle tracking (19). Because the only required equipment to perform EWI is a clinical ultrasound scanner (20), the technique is also highly translational. The EWI images are currently generated off-line on a personal computer workstation within 10 min or less but could be implemented in real time on most modern clinical scanners. The EW was first depicted on EWI cine loops in canines (21) and humans (22), its correlation with conduction velocities was verified in mice (23), and, more recently, EWI was shown to be capable of mapping intermediate and acute ischemia in canines (16). Additionally, the EW was reproduced in a simulation model where it was shown to be correlated with the electrical activation times (24).

Previous work has established a link between the electrical and electromechanical activation at the tissue level using invasive and noninvasive methods. In ref. 13, Badke et al. used implanted ultrasonic crystals and electrodes in canines during atrial, right-ventricular (RV), left-ventricular-apical (LVa) and left-ventricular-basal (LVb) pacing, and found a slope of 1.1 ($r = 0.91$) between the electrical and electromechanical activation times. In ref. 14, Wyman et al. used high temporal resolution MR tagging and bipolar electrodes during RV apical (RVa) and LVb pacing in canines and found a slope of 1.06. These results suggest that the electrical activation sequence could be deduced from the electromechanics. However, as of today, EWI has yet to be directly linked to the underlying electrophysiology.

EWI is hereby found to be capable of noninvasively and accurately localizing the pacing origins and obtaining high-resolution, transmural maps of the electromechanical activation sequence along various ventricular planes. For the purpose of this validation study, bipolar electrodes were implanted in open-chest canine hearts to pace the heart and simultaneously map the activation times with EWI. The region of earliest activation in the EWI isochrones accurately matched the location of the pacing electrode. The activation sequences obtained with EWI and electrography were shown to be in excellent agreement, confirming that electrical events in the heart can be noninvasively inferred by using customized clinical ultrasound systems. Finally, we show noninvasive feasibility of EWI in the entire hearts of two normal human subjects.

Results

To establish the feasibility of studying electrical cardiac events using EWI, canine hearts were imaged in vivo during sinus rhythm and four distinct epicardial pacing protocols as follows: (*i*) from the basal region of the lateral wall (LVb), (*ii*) from the LVa, (*iii*) from the apical region of the anterior-lateral wall of the left ventricle (LVar), and (*iv*) from the apical region of the lateral wall of the right ventricle (RVa). Bipolar electrograms were also acquired simultaneously in two canines. The EWI flowchart is illustrated in Fig. 1. The full view of the heart is first divided into sectors (Fig. 1*A*) for which RF signals are acquired (Fig. 1*B*) during separate heartbeats. Displacements are then estimated along the ultrasound beam (Fig. 1*C*) and used to reconstruct the full view of the heart (Fig. 1*D*). Finally, interframe strains are estimated along the ultrasound beam and segmented (Fig. 1*E*). Isochrones of the EW can then be displayed in 3D space by combining multiple views (Fig. 1*F*).

Two standard image planes, identical to the apical four- and two-chamber views used in echocardiography, were selected. The alignment of those two planes in a biventricular view using anatomical landmarks such as the apex allowed a three-dimensional depiction of the EW propagation (Fig. 2). Fig. 2 and the corresponding Movie S1 depict the propagation of the EW at different time points following pacing from the basal region of the lateral wall (Fig. 2 *A*–*E*), as indicated on the ECG (Fig. 2*F*). Colors correspond to extension (red) and compression (blue) of the myocardial tissue along the direction of the ultrasound beam.

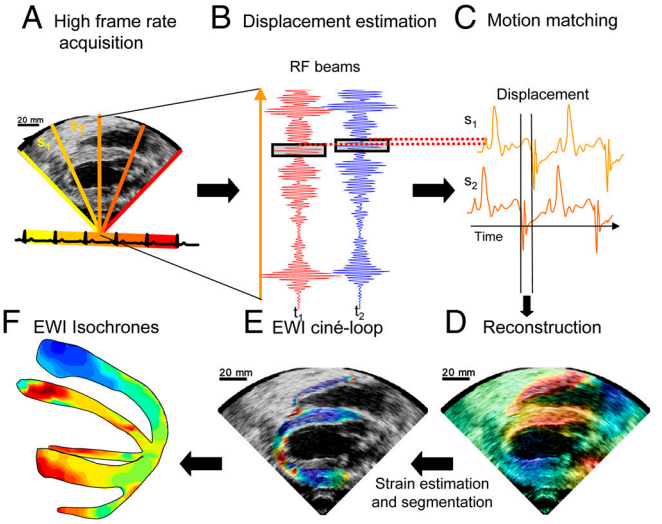

Fig. 1. Block diagram of the EWI technique. (*A*) A full view of the two ventricles is first divided in partially overlapping sectors, which are imaged at separate heartbeats. (*B*) High-precision displacement estimation between two consecutively acquired RF beams (t_1, t_2) is then performed using very high-frame-rate RF speckle tracking. (*C*) A region of the heart muscle, common to two neighboring sectors, is then selected. By comparing the temporally varying displacements measured in neighboring sectors (s_1, s_2) via a cross-correlation technique, the delay between them is estimated. (*D*) A full-view cine loop of the displacement overlaid onto the B mode can then be reconstructed with all the sectors in the composite image synchronized. (*E*) The heart walls are then segmented, and incremental strains are computed to depict the EW. (*F*) By tracking the onset of the EW, isochrones of the sequence of activation are generated.

Because of the positioning of the ultrasound probe during those experiments, the interframe strain (referred to simply as "strain" for brevity purposes) estimation was performed mostly in the radial direction, except in the apical region of the anterior and lateral walls where the estimation was performed longitudinally. The radial, circumferential, and longitudinal directions are depicted in Fig. S1. In simple terms, after a certain wall region is electrically activated to undergo systole, it is expected to transition from radial thinning to thickening and from longitudinal lengthening to shortening. This is depicted in Fig. 2: 15 ms after pacing (Fig. 2*A*), the tissue has not started to contract yet because of the electromechanical delay existing between the onset of the action potential and the contraction at the cellular level (1, 3).

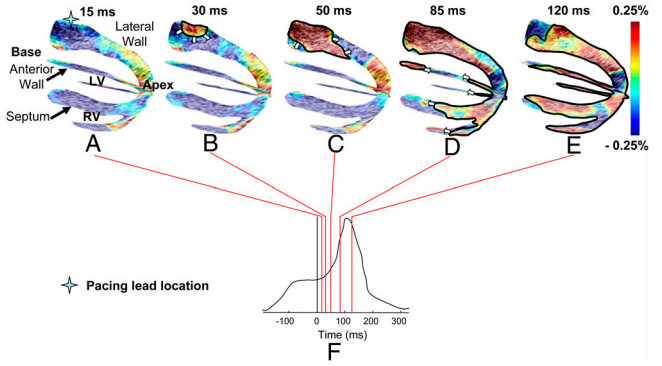

Fig. 2. Propagation of the EW when paced from the lateral wall, near the base. Activated regions are traced at (*A*) 15 ms, (*B*) 30 ms, (*C*) 50 ms (*D*) 85 ms, and (*E*) 120 ms and indicated on the (*F*) ECG; 0 ms corresponds to the pacing stimulus. (*A*–*C*) The EW propagates from the basal part of the lateral wall toward the apex. (*D*) Note that in the apical region, a transition from lengthening to shortening is observed rather than a transition from thinning to thickening. (*D*–*E*) In the anterior wall, the EW propagates from both the base and apex. The scale shows interframe strains.

Radial thinning and longitudinal lengthening are observed. At 30 ms, thickening near the pacing lead (Fig. 2*B*) in the basal region of the lateral wall is observed, while the other regions of the ventricles undergo negligible strain variations. This initial thickening region then extends (Fig. 2*C*) and reaches the apical region of the lateral, septal, anterior, and right-ventricular walls as well as the basal region of the anterior wall (Fig. 2*D*). Note that in the apical region of the anterior and lateral walls, activation resulted in shortening (blue). At 120 ms, both ventricles were activated except for a small region in the anterior and posterior walls near the base.

Isochronal maps were obtained by defining the onset of the EW as the first time point following the Q wave at which the temporal strain profile crosses zero (16). Because interframe strains are used, a change in the sign of those strains (or in other terms, their zero-crossing) corresponds to a change in the behavior of the tissue; i.e., the tissue transitions from a relaxing to a contracting state. Fig. 3 shows such maps during four different pacing schemes in both anterior and posterior views, i.e., LVb (Fig. 3*A* and Movie S1), LVa (Fig. 3*B* and Movie S2), LVar (Fig. 3*C* and Movie S3), and RVa (Fig. 3*D* and Movie S4). In three cases (Fig. 3 *A*, *B*, and *D*), we identified a unique origin of the EW (i.e., the region with the shortest zero-crossing time). This region coincided with the position of the pacing lead. When pacing from the apical region of the antero-lateral wall (Fig. 3*C*), the pacing lead was located in the apical region between the two planes. A clear propagation of the EW emanating from the location of the lead was depicted. The same results were obtained in two separate animal cases (Fig. 3 *A*, *B*, *D* and *C*, respectively) indicating preliminary reproducibility of the method.

During sinus rhythm, the natural pacemaker is the sinus node, located in the right atrium. Signals are generated spontaneously at the sinus node, travel through the atrium (during the P wave), to the atrio-ventricular node, the bundle of His, and finally to the Purkinje fiber network and the ventricular myocardium (during the QRS complex). Complex activation patterns are expected when imaging the ventricles, because activation will originate from multiple locations following the Purkinje fiber network. Fig. 3*E* (corresponding to Movie S5) shows the isochronal representation of the EW in the left and right ventricles during sinus rhythm. Early activation at the median level and late activation at the basal and apical levels was observed. Activation of the right-ventricular wall occurred after activation of the septal and lateral walls in both cases. Therefore, the EWI isochrones during sinus rhythm exhibited multiple origins of propagation (i.e., early activated regions) rather than a unique origin observed when pacing from a single lead.

In order to compare the EW against the electrical activation, four recording bipolar electrodes were implanted in the two-chamber view plane (Fig. S1). Fig. 4 shows the time of electrical activation and the corresponding EW onset time. The EW onset time was obtained by averaging the isochrones within the echocardiographic segments (mean ± temporal standard deviation within a cardiac segment). The electrical activation times were averaged over ten cardiac cycles (mean ± temporal standard deviation). A linear relationship between the EW onset and the electrical activation time was found (Fig. 4) in all four pacing cases and during sinus rhythm with a slope of 0.99 ± 0.1 ($R^2 = 0.88$, $p < 10^{-7}$) and an intercept of 14 ± 7 ms ($p = 0.06$).

In the human feasibility study, the four-chamber view is imaged from the apex. In that view, longitudinal strains are mapped in most of the heart. Activation results mostly in myocardial shortening (blue) of the tissue, both in the atria and the ventricles. Fig. 5*A* (corresponding to Movie S6) shows the EW in a 23-y-old healthy female; strains lower than 0.025% were not displayed. When mapping the EW in the canine ventricles, we observed a transition from negative (or positive) strains to positive (or negative) strains, most likely because the ventricles were prestretched during atrial contraction or not fully relaxed because of relatively high pacing rates. In the atria of normal human subjects, strains were very close to zero before the P wave. This is expected, because the heart rate of the subjects observed was low (50–60 beats per minute). Therefore, unlike in the ventricle case, a transition from relaxation (negative or positive strain, respectively) to contraction (positive or negative strain, respectively) was not detected in the atria. In the atria, activation resulted instead in a transition from strains close to zero to positive (or negative) strains. The time of activation in the atria was defined as the first occurrence following the onset of the P wave at which the strains in absolute value exceeded 0.025%. This threshold was chosen to account for the presence of noise and corresponds to approximately one-tenth of the order of magnitude of strains observed during the electrical activation. Using this definition, the right atrium was activated 30–35 ms following the onset of the P wave, and the electromechanical activation propagated toward the left atrium. Shortening of the atria also resulted in lengthening of the still passive, inactivated ventricles. As a result, immediately after the onset of the Q wave, the ventricles were in a relaxation (or prestretched) state. The septum was activated first at the midlevel, and the EW propagated toward the apex and base. Fig. 5*B* shows the corresponding isochronal representation of the EW. Similar results were observed in a 23-y-old male subject (Fig. S2 and Movie S7). An alternative representation of these two cases, showing only the electromechanical activation after filtering of the passive behavior of the heart, is also provided (Movies S8 and S9, respectively). This was performed by inverting the sign of the strains in ventricular

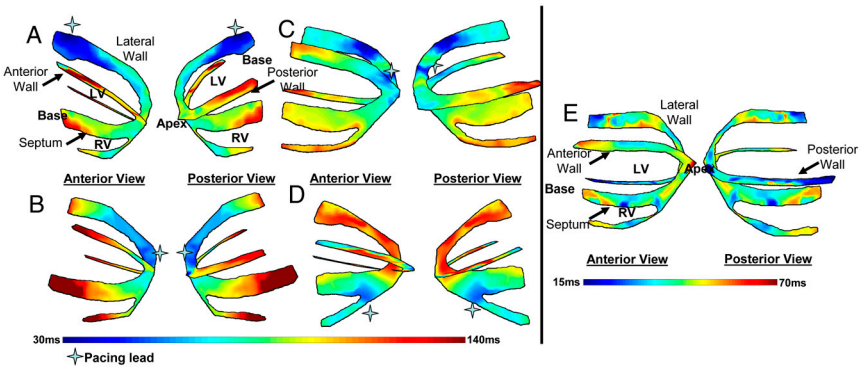

Fig. 3. Isochrones showing the activation sequence under different pacing protocols. (*A*) Pacing from the basal region of the lateral wall. (*B*) Pacing from the apex. (*C*) Pacing from the apical region of the lateral wall. (*D*) Pacing from the apical region of the right-ventricular wall. (*E*) Isochrones showing the EW activation sequence during sinus rhythm. The activation sequence exhibits early activation at the median level and late activation at the basal and apical levels. Activation of the right-ventricular wall occurred after the activation of the septal and lateral walls.

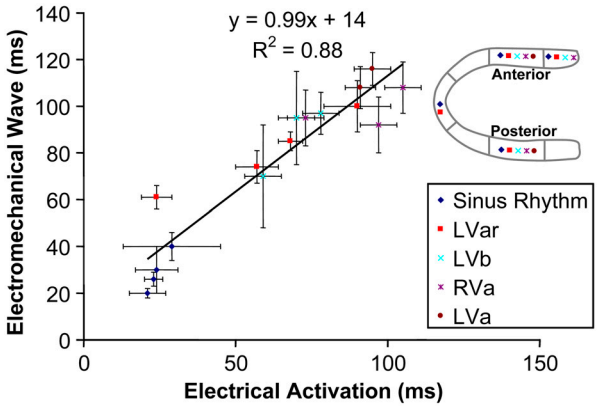

Fig. 4. Electrical and electromechanical activation times during the four pacing protocols and sinus rhythm in four different heart segments in the posterior and anterior walls, as indicated in the legend. A strong correlation was observed, with a slope of 0.99.

regions showing negative strains (compression) at the onset of the QRS complex.

Discussion

The objectives in this study were to determine the accuracy and reliability of EWI in depicting electromechanical events in the heart and to demonstrate feasibility in humans.

EWI was performed in canine hearts during four distinct pacing protocols and sinus rhythm. Isochronal maps of the EW onset were generated, and the earliest activation region was found to be highly correlated with the pacing site location. Electrodes were also implanted in the heart, allowing simultaneous measurements of the electrical activation times in selected echocardiographic segments of the heart. A linear relationship was found between the electrical activation times and the EW onset, thereby showing that at the scale of the cardiac segments, the EW follows the electrical activation sequence. The validation of the link between the EW and the electrical activation sequence in canines was twofold. First, the localization of the earliest activation time in the EWI isochrones was highly correlated with the pacing site, thus allowing the noninvasive identification of the pacing lead location. For instance, right-ventricular pacing (Fig. 3*D*) could easily be distinguished from left-ventricular free wall pacing, apical pacing, or sinus rhythm. Moreover, the EWI isochrones obtained during sinus rhythm (Fig. 3*E*) were in agreement with maps previously reported in the literature, which were obtained using electrography (25–27). Second, the electrical activation times and the EWI isochrones where highly correlated, with a slope of 0.99 (Fig. 4). Other groups have reported similar findings in vivo; i.e., a linear relationship between mechanical and electrical activations, with slopes of 1.1 (13), 1.06 (14), and 0.87–1.05 (28). This suggests that EWI could potentially become a noninvasive tool to map the electrical activation sequence. The minimum requirement for this to happen would be to obtain a monotonic relationship between the maps of electrical and electromechanical activation times. Comparing such maps, however, poses a significant challenge. The electrodes affect both the mechanical and electrical behavior of the heart muscle and can also generate artifacts on the ultrasound image. To circumvent this issue in this study, the imaging plane was selected in the vicinity of the plane defined by the electrode locations without being affected by the aforementioned artifacts. This approach showed that, at least on the scale of the heart segments in the regions studied, EWI reflects the electrical activity with accuracy. Further studies are needed, however, to establish at which resolution and under which physiological conditions this relationship is maintained. The observed propagation from the epicardium to the endocardium during pacing (e.g., Fig. 2 *A*–*C*) indicates that EWI also provides information about the transmural electrical activity, which was also confirmed in simulations (29). However, in sinus rhythm, activation from endocardium to epicardium, which is expected, was not observed everywhere in the heart. This could be explained by the limited information obtained through 2D observation of an inherently 3D phenomenon such as the cardiac electrical activation in combination with the fact that strain measurements at the boundary of the heart wall are more susceptible to noise. Generalizing EWI to three dimensions could help in addressing those issues.

The EW was observed in the normal human atria (Fig. 5) and, although no validation with electrodes was provided in the atria in the current study, followed the expected electrical activation sequence in two human subjects. The earliest activation region was located in the right atrium, where the sinus node is located. Activation propagated in the atria during the P wave. Following the onset of the QRS complex, activation in the ventricles was observed in multiple regions near the midlevel, in agreement with previous ex vivo studies of the activation sequence in human hearts based on electrography (25). To our knowledge, the normal transmural electrical activation sequence in conscious subjects is not available in the literature. The electrical activation sequence in humans was initially obtained in isolated hearts (25) or during intraoperative mapping studies under nonphysiological conditions. More recently, the epicardial electrical activation sequence was obtained in the normal human heart under complete physiological conditions (30). However, such an approach is limited to the epicardium and thus cannot be used to map the endocardium or the septum, nor can it be used across the thickness of the heart walls. EWI might thus constitute an important complementary tool to the ECG to assess the normal electrical activation sequence in normal subjects.

Moreover, when the function of a region of the heart is compromised, both the normal electrical and mechanical behaviors of the heart can be altered. For example, scars following a myocardial infarction can lead to the formation of reentry circuits overriding the sinus node as the heart pacemaker and resulting

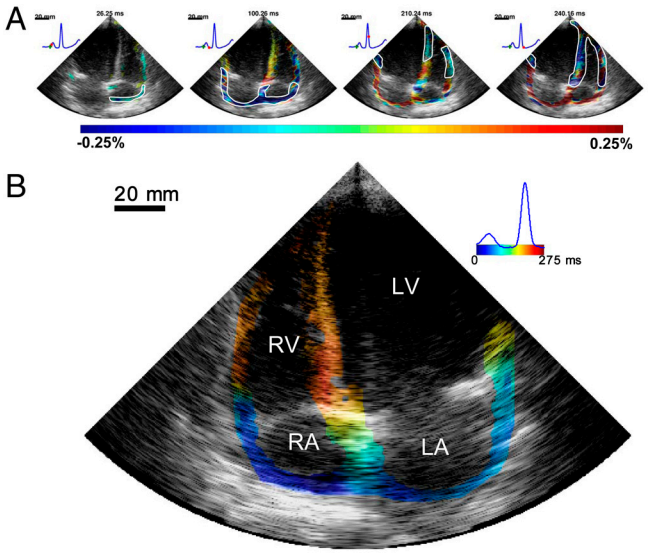

Fig. 5. Normal sinus rhythm in a healthy volunteer (23 y-old female). (*A*) The EW first occurred in the right atrium and propagated toward the left atrium (blue). This resulted in prestretching of the ventricles (red). The EW then appeared at the midlevel in the septum and close to the apex in the right-ventricular wall, and then propagated toward the apex and the base. (*B*) Corresponding isochrones. The earliest activation occurred in the right atrium. In the ventricles, it was possible to identify multiple regions of early activation, namely at the midlevel of the septum, near the apex of the right ventricle, and close to the base in the lateral wall. RA, right atrium; LA, left atrium.

in ventricular tachycardia or fibrillation. A scar could also result in an asynchronous electrical activation of the ventricles, which over time triggers remodeling of the heart and eventually leads to heart failure; i.e., the heart becomes incapable of providing sufficient blood flow to the rest of the body. Such diseases can currently be treated, e.g., by neutralizing the arrhythmogenic zones through ablation or by resynchronizing the contraction of both ventricles through cardiac resynchronization therapy. Although both ablation and biventricular pacing therapies are routinely used, they are yet to be fully understood and optimized, mostly because of the challenges associated with mapping the electrical activity of the heart. Over the past several decades, efforts have been aimed at the development of technologies to map the cardiac electrical activation. Minimally invasive procedures where a catheter containing one or several electrodes is inserted into the heart chambers are now frequently used in the clinic. These clinical procedures are, however, limited to conditions where ablation therapy is indicated. Effectively, they are not used routinely for diagnosis or to optimize the lead placement and timings of pacing therapies. They are also limited to the endocardium, hence requiring an additional procedure when the region to ablate is located on the epicardium. A number of minimally invasive or noninvasive technologies have been developed to tackle those limitations. Typically, these methods are based on measurements performed outside of the myocardium, e.g., on the body surface (4, 5) or inside the heart cavities (7). From these measurements, an inverse problem that requires accurate knowledge of the geometry of the organs and structures located at and between the measurement surface and the heart muscle then needs to be solved. For example, newly developed electrocardiographic imaging methods based on high-density body surface potential maps are most promising (4, 5) and clinically relevant (6, 31) in that regard. Although possessing undeniable qualities, these methods require either ionizing exposure [i.e., three-dimensional computed tomography (5)] or MRI (6), which can be contraindicated for patients with pacemakers or stents. EWI could constitute an interesting alternative or complementary approach to those technologies, as it can be used in real time, at the point of care and can be easily integrated into existent ultrasound systems and current clinical protocols at no or low additional cost.

The necessary assumption in using EWI for the study of the electrical function of the heart is that the electrical and electromechanical activation times remain correlated. This assumption may no longer be valid when the myocardial contractility is severely compromised. However, because EWI is a direct method, the displacements and strains measured during the QRS complex remain accurate in pathological regions and can be used to identify the extent of the problem, e.g., ischemia (16). Moreover, the RF signals acquired at very high frame rates for EWI can also be processed in order to map more standard measures at higher accuracy, such as cumulative systolic strains, which can also be used, e.g., to identify or confirm ischemic or infarcted zones (32, 33). Some of the methods shown in this paper could also be improved. For example, isochrones were obtained manually and thus depend on the user. Given the current noise level present in the EWI images, manual selection of pixels to map to avoid spurious data was necessary to provide a continuous depiction of the general EW propagation pattern. This approach can, however, introduce user-dependent bias in the method; therefore, automatic generation of isochronal representations would benefit EWI. This is part of an ongoing effort by our group. On the other hand, the EW cine loops themselves can be used for diagnosis, and are user-independent. The number of subjects scanned in this study was limited. A larger sample size will be necessary to thoroughly quantify the resolution, accuracy, and reproducibility of EWI for electrical mapping. For example, the regression of Fig. 4 does not have the required population sample to quantify the slope of the electromechanical relationship for each individual pacing scheme separately, and the electrical and electromechanical activation times used were averaged over relatively large (approximately 1 cm) regions. For example, a monotonic relationship was not observed in the RVa case. Finally, the threshold used when mapping human subjects with EWI was chosen to be one-tenth of the order of magnitude of the strains measured during the electrical activation (i.e., 0.025%); further studies are necessary to fully assess the influence of this parameter.

In summary, EWI may constitute a unique tool for evaluating the cardiac electromechanical function of a patient at the point of care and in real time. The ubiquity of ultrasound scanners in diagnostic cardiology indicate the important translational potential of EWI for screening as well as diagnostic and treatment monitoring in cardiology.

Methods

Experimental Protocol. In this study, approved by the Institutional Animal Care and Use Committee of Columbia University, three ($n = 3$) mongrel dogs of either sex, ranging from 23 to 32 kg in weight, were anesthetized with an intravenous injection of thiopental (10–17 mg/kg). All animals were mechanically ventilated with a rate- and volume-regulated ventilator on a mixture of oxygen and titrated isoflurane (0.5–5.0%). Morphine (0.15 mg/kg, epidural) was administered before surgery, and lidocaine (50 mg/kg per h, intravenous) was used during the whole procedure. To maintain blood volume, 0.9% saline solution was administered intravenously at 5 mL/kg per h. The animals were positioned supine on a heating pad throughout the entire procedure (to avoid hypothermia).

Standard limb leads were placed for surface ECG monitoring. Solid-state pressure transducer catheters (Millar Instruments) were inserted into the left-ventricular cavity via the right carotid artery and in the aorta. Oxygen saturation of the blood and peripheral blood pressure were monitored throughout the experiment.

The chest was opened by lateral thoracotomy using electrocautery. After removal of the pericardium, up to twelve sonomicrometry crystals with a 2-mm diameter combined with bipolar electrodes were then implanted in the ventricles. Sonomicrometry signals were not used for the purpose of this study and were turned off when ultrasound images were acquired. For endocardial and midwall crystals, an 18G needle was used for insertion. All crystals were maintained in position after placement using silk sutures. Pacing and electrophysiology measurements were performed using the same crystals. Recording electrodes were located in the midwall along the two-chamber view, and pacing electrodes were located on the epicardium along the four-chamber view (Fig. S1). The time of electrical activation was determined by identifying the maximum value of the bipolar electrode signal. Because unipolar and bipolar potential mapping have been shown to be nearly identical (34), bipolar mapping was preferred to allow the use of identical electrodes for pacing or recording and to avoid difficulties such as far-field potentials.

The human subject study protocol was approved by the Institutional Review Board of Columbia University, and informed consent was obtained from all human subjects prior to scanning. For this feasibility study, two normal subjects were imaged: a 23-y-old female and a 23-y-old male.

Echocardiography In canines, an Ultrasonix RP system with a 3.3-MHz phased array was used to acquire RF frames from 390 to 520 fps using an automated composite technique (20). Briefly, to increase the resulting frame rate, the image was divided into partially overlapping sectors corresponding to separate cardiac cycles (Fig. 1*A*). To minimize motion artifacts, the probe was attached to a stabilizer (Medtronic Corp.) and the respirator was interrupted for 6–20 s depending on the acquisition. The axial incremental displacements were obtained with an RF-based cross-correlation method (Fig. 1*B*) (window size: 4.6 mm, 80% overlap). Briefly, this method consists in dividing every ultrasound beam in a large number of overlapping, one-dimensional, 4.6-mm-long windows. Then, the following process is applied to each window and each sampled time t. A reference window at time t is compared with all the windows contained in the same beam at sampled time $t + 1$. The axial location of the window providing the highest correlation determines the axial displacement between two consecutive sampled times. After repeating this process for every available window and every available sampled time, we obtain axial displacements at multiple locations along the ultrasound beam and for every sampled time. The full-view image was then reconstructed using the motion-matching technique (Fig. 1*C*) (16). Briefly, this method consists of comparing, through a cross-correlation method,

the incremental displacements measured in the overlapping line of two sectors obtained at different heartbeats to synchronize the sectors. More specifically, the acquisition sequence is designed such that each sector contains at least one ultrasound beam that is also part of the following sector. Therefore, this overlapping beam is expected to result in identical (or highly similar) axial displacements whether they corresponds to heartbeat h that occurred when sector s was acquired or to heartbeat $h+1$ that occurred when sector $s+1$ was acquired. By comparing, over time, the displacements obtained in the overlapping beams, one can obtain the time delay corresponding to the maximum cross-correlation coefficient to synchronize each set of neighboring sectors. The procedure is repeated for each pair of sectors, allowing the reconstruction of the full-view of the heart, hence ensuring the continuity of the transition incremental displacements across sectors. This method does not rely on the ECG. Therefore, it is especially useful in cases where the ECG may be unavailable or too irregular to perform ECG gating (16). The axial incremental strains were then obtained by taking the spatial derivative of incremental strains in the axial direction using a least-squares estimator (35) with a kernel equal to 6.75 mm (Fig. 1*D*). The myocardium was segmented using an automated contour tracking technique (36), and displacement and strain maps were then overlaid onto the corresponding B-mode images (Fig. 1*E*). In this study, we considered incremental strains in the Eulerian description (37); i.e., the local change in length was measured with respect to the previous frame in a fixed coordinate system. Isochrones were generated by mapping the first time at which the incremental strains crossed zero following the Q wave. More specifically, the absolute value of the incremental strains was minimized in a temporal window following the Q wave in up to 100 manually selected regions. Noisy data were excluded. Subsample resolution was obtained through spline interpolation, and Delaunay interpolation was used to construct continuous isochronal maps. Two echocardiographic planes, identical to the planes imaged in the standard apical four- and two-chamber views, were imaged across the long axis of the heart. These two views were temporally coregistered using the ECG signals, spatially coregistered by an echocardiography expert, and displayed in a three-dimensional biplane view in Amira 4.1 (Visage Imaging) (Figs. 1*F* and 2). In humans, the same acquisition sequence and algorithms were used, with the exception that acquisition was performed using an Ultrasonix MDP system. The least-square estimator kernel size was equal to 5.22 mm. To generate videos showing only electromechanical activation (Movies S8 and S9), the sign of the strains was inverted in the regions showing negative strains (compression) at the onset of the QRS complex. Following this operation, strains larger than −0.025% were not shown. Whenever necessary to reduce registration artifacts, subjects were asked to hold their breath for up to 18 s.

ACKNOWLEDGMENTS. The authors thank Edward Ciaccio, Eiichi Hyodo, Asawinee Danpinid, Aram Safarov, and Ihsaan Sebro for their help during experiments and Heather S. Duffy, Peter Danilo, and Iryna N. Shlapakova for their advice on the experimental procedure. The authors also thank Jianwen Luo, Stanley J. Okrasinski, and Viatcheslav Gurev for helpful discussions, Grace Kiser for editing advice, Shinichi Iwata for scanning human subjects, and Dr. Shunichi Homma for his guidance in the echocardiography scanning efforts. This study was supported in part by the National Institutes of Health (R01EB006042, R21HL096094) and Wallace H. Coulter Foundation. J.P. was funded in part by the Natural Sciences and Engineering Research Council of Canada and by the Fonds Québécois de la Recherche sur la Nature et les Technologies.

1. Bers DM (2002) Cardiac excitation-contraction coupling. *Nature* 415:198–205.
2. Ashikaga H, et al. (2007) Transmural dispersion of myofiber mechanics: Implications for electrical heterogeneity in vivo. *J Am Coll Card* 49:909–916.
3. Cordeiro JM, Greene L, Heilmann C, Antzelevitch D, Antzelevitch C (2004) Transmural heterogeneity of calcium activity and mechanical function in the canine left ventricle. *Am J Physiol Heart Circ Physiol* 286:H1471–H1479.
4. Zhang X, et al. (2005) Noninvasive three-dimensional electrocardiographic imaging of ventricular activation sequence. *Am J Physiol Heart Circ Physiol* 289:H2724–H2732.
5. Ramanathan C, Ghanem RN, Jia P, Ryu K, Rudy Y (2004) Noninvasive electrocardiographic imaging for cardiac electrophysiology and arrhythmia. *Nat Med* 10:422–428.
6. Berger T, et al. (2006) Single-beat noninvasive imaging of cardiac electrophysiology of ventricular pre-excitation. *J Am Coll Card* 48:2045–2052.
7. Schilling RJ, Peters NS, Davies DW (1998) Simultaneous endocardial mapping in the human left ventricle using a noncontact catheter: Comparison of contact and reconstructed electrograms during sinus rhythm. *Circulation* 98:887–898.
8. Tavarozzi I, et al. (2002) Magnetocardiography: Current status and perspectives. Part II: Clinical applications. *Ital Heart J* 3:151–165.
9. Greenstein JL, Hinch R, Winslow R (2006) Mechanisms of excitation-contraction coupling in an integrative model of the cardiac ventricular myocyte. *Biophys J* 90:77–91.
10. Rice JJ, Wang F, Bers DM, de Tombe PP (2008) Approximate model of cooperative activation and crossbridge cycling in cardiac muscle using ordinary differential equations. *Biophys J* 95:2368–2390.
11. Campbell SG, Flaim SN, Leem CH, McCulloch AD (2008) Mechanisms of transmurally varying myocyte electromechanics in an integrated computational model. *Philos Transact A Math Phys Eng Sci* 366:3361–3380.
12. Gurev V, Constantino J, Rice JJ, Trayanova N (2010) Distribution of electromechanical delay in the heart: Insights from a three-dimensional electromechanical model. *Biophys J* 99:745–754.
13. Badke FR, Boinay P, Covell JW (1980) Effects of ventricular pacing on regional left ventricular performance in the dog. *Am J Physiol Heart Circ Physiol* 238:H858–H867.
14. Wyman BT, Hunter WC, Prinzen FW, McVeigh ER (1999) Mapping propagation of mechanical activation in the paced heart with MRI tagging. *Am J Physiol Heart Circ Physiol* 276:H881–H891.
15. Prinzen FW, et al. (1992) The time sequence of electrical and mechanical activation during spontaneous beating and ectopic stimulation. *Eur Heart J* 13:535–543.
16. Provost J, Lee W, Fujikura K, Konafagou E (2010) Electromechanical wave imaging of normal and ischemic hearts in vivo. *IEEE Trans Med Imaging* 29:625–635.
17. Shehata M, Cheng S, Osman N, Bluemke D, Lima J (2009) Myocardial tissue tagging with cardiovascular magnetic resonance. *J Cardiovasc Magn Reson* 11:55.
18. Zwanenburg JJM, et al. (2004) Timing of cardiac contraction in humans mapped by high-temporal-resolution MRI tagging: Early onset and late peak of shortening in lateral wall. *Am J Physiol Heart Circ Physiol* 286:H1872–H1880.
19. Walker W, Trahey G (1994) A fundamental limit on the performance of correlation based phase correction and flow estimation techniques. *IEEE Trans Ultrason Ferroelectr Freq Control* 41:644–654.
20. Wang S, Lee W, Provost J, Luo J, Konofagou EE (2008) A composite high-frame-rate system for clinical cardiovascular imaging. *IEEE Trans Ultrason Ferroelectr Freq Control* 55:2221–2233.
21. Pernot M, Konofagou EE (2005) Electromechanical imaging of the myocardium at normal and pathological states. *Proceedings of the 2005 IEEE Ultrasonics Symposium* (Institute of Electrical and Electronic Engineers, New York) pp 1091–1094.
22. Pernot M, Fujikura K, Fung-Kee-Fung SD, Konofagou EE (2007) ECG-gated, mechanical and electromechanical wave imaging of cardiovascular tissues in vivo. *Ultrasound Med Biol* 33:1075–1085.
23. Konofagou EE, et al. (2007) Noninvasive electromechanical wave imaging and conduction velocity estimation in vivo. *Proceedings of the 2007 Ultrasonics Symposium* (Institute of Electrical and Electronic Engineers, New York) pp 969–972.
24. Provost J, Gurev V, Trayanova N, Konofagou EE (2011) Mapping of cardiac electrical activation with electromechanical wave imaging: An in silico–in vivo reciprocity study. *Heart Rhythm* 8:752–759.
25. Durrer D, et al. (1970) Total excitation of the isolated human heart. *Circulation* 41:899–912.
26. Sengupta PP, Tondato F, Khandheria BK, Belohlavek M, Jahangir A (2008) Electromechanical activation sequence in normal heart. *Heart Fail Clin* 4:303–314.
27. Scher AM, Young AC (1956) The pathway of ventricular depolarization in the dog. *Circ Res* 4:461–469.
28. Faris OP, et al. (2003) Novel technique for cardiac electromechanical mapping with magnetic resonance imaging tagging and an epicardial electrode sock. *Ann Biomed Eng* 31:430–440.
29. Gurev V, Provost J, Konofagou EE, Trayanova N (2009) In silico characterization of ventricular activation pattern by electromechanical wave imaging. *Heart Rhythm Suppl* 6:S357.
30. Ramanathan C, Jia P, Ghanem R, Ryu K, Rudy Y (2006) Activation and repolarization of the normal human heart under complete physiological conditions. *Proc Natl Acad Sci USA* 103:6309–6314.
31. Ghosh S, Rhee EK, Avari JN, Woodard PK, Rudy Y (2008) Cardiac memory in patients with Wolff-Parkinson-White syndrome: Noninvasive imaging of activation and repolarization before and after catheter ablation. *Circulation* 118:907–915.
32. Lee W, et al. (2007) Theoretical quality assessment of myocardial elastography with in vivo validation. *IEEE Trans Ultrason Ferroelectr Freq Control* 54:2233–2245.
33. Lee W, Provost J, Fujikura K, Wang J, Konofagou EE (2011) In vivo study of myocardial elastography under graded ischemia conditions. *Phys Med Biol* 56:1155–1172.
34. Kimber S, et al. (1996) A comparison of unipolar and bipolar electrodes during cardiac mapping studies. *Pacing Clin Electrophysiol* 19:1196–1204.
35. Kallel F, Ophir J (1997) A least-squares strain estimator for elastography. *Ultrason Imaging* 19:195–208.
36. Luo J, Konofagou EE (2008) High-frame rate, full-view myocardial elastography with automated contour tracking in murine left ventricles in vivo. *IEEE Trans Ultrason Ferroelectr Freq Control* 55:240–248.
37. Lai WM, Rubin D, Krempl E (1993) *Introduction to Continuum Mechanics* (Pergamon, Oxford), 3rd Ed.